

# Free Space Optical Communication with Spatial Modulation and Coherent Detection over Atmospheric Turbulence Channels

Kostas P. Peppas, *Senior Member, IEEE* and P. Takis Mathiopoulos, *Senior Member, IEEE*

arXiv:1503.02831v1 [cs.IT] 10 Mar 2015

**Abstract**—In this paper, the use of optical spatial modulation (OSM), which has been recently emerged as a power and bandwidth efficient pulsed modulation technique for indoor optical wireless communication, is proposed as a simple, low-complexity means of achieving spatial diversity in coherent free space optical (FSO) communication systems. In doing so, this paper makes several novel contributions as follows. Firstly, it presents a very generic mathematical framework for obtaining the Average Bit Error Probability (ABEP) of uncoded OSM in the presence of turbulence induced fading. Although the proposed framework is general enough to accommodate any type of models based on turbulence scattering, here we focus on the H-K distribution, as the adopted atmospheric turbulence channel model. This framework is exact for MIMO systems with two transmit and an arbitrary number of receive apertures. For OSM systems with an arbitrary number of transmit apertures, tight bounds for the ABEP are also proposed. Secondly, for convolutional coded OSM systems, tight upper bounds for the ABEP are derived. Various numerical performance evaluation results are also presented and compared with equivalent results obtained by Monte Carlo simulations which verify the accuracy of the analytical expressions.

**Index Terms**—average bit error probability, atmospheric turbulence, coherent detection, free space optical communication systems, H-K distribution, multiple-input multiple-output (MIMO) systems, optical spatial modulation.

## I. INTRODUCTION

Free-space optical (FSO) communication systems have recently attracted great attention within the research community as well as for commercial use. FSO systems can provide ultra-high data rates (at the order of multiple gigabits per second), immunity to electromagnetic interference, excellent security and large unlicensed bandwidth i.e. hundred and thousand times higher than radio-frequency (RF) systems, along with low installation and operational cost [2]–[4]. Because of their attractive features, FSO communication systems are today used for a wide variety of applications including "last mile" access, back-haul for wireless cellular networks, fiber backup, HDTV transmission, disaster recovery and rescue operations [3].

K. P. Peppas is with the Department of Informatics and Telecommunications, University of Peloponnese, 22100 Tripoli, Greece. He is also with the Institute of Informatics and Telecommunications, National Centre for Scientific Research—"Demokritos," Patriarhou Grigoriou and Neapoleos, 15310 Agia Paraskevi, Athens, Greece (e-mail: kpeppas@iit.demokritos.gr)

P. T. Mathiopoulos is with the Department of Informatics and Telecommunications, National and Kapodistrian University of Athens, 15784 Zografou, Athens, Greece (e-mail: mathio@di.uoa.gr).

The challenge in employing such systems is that FSO links are highly vulnerable due to the detrimental effects of attenuation under adverse weather conditions (e.g. fog), pointing errors and atmospheric turbulence. Turbulence induced fading, also known as scintillation in optical communication terminology, results in time-varying fluctuations in the irradiance of the received optical laser beam in a similar fashion as fading in RF systems [4]. One method to improve the reliability of the FSO link is to employ spatial diversity, namely multiple-lasers and multiple-apertures to create a multiple-input multiple-output (MIMO) optical channel. Because of its low complexity, spatial diversity is a particularly attractive fading mitigation technique and performance enhancements have been extensively studied in many past research works [5]–[14].

In order to evaluate the impact of atmospheric turbulence on the performance of OSM, accurate models for the fading distribution are necessary. For example the lognormal distribution is often used to model weak turbulence conditions whereas the negative exponential and the K-distribution are used to model strong turbulence conditions [15]. Universal statistical models have also been proposed to model scintillation over all turbulence conditions, including the gamma-gamma [16], the lognormal-Rice (or Beckmann) [17] the homodyned K distribution (H-K) [18] and the I-K [7], [19]–[22] distributions. All these three models are based on the argument that scintillation is a doubly stochastic random process modelling both small and large scale turbulence effects. Besides, they agree well with measurement data and simulations for a wide range of turbulence conditions.

In this paper, the H-K distribution is adopted to model turbulence-induced fading. The main reason for this choice is the fact that this distribution is based on a very general scattering model which is valid for a wide range of atmospheric conditions. It is also noted that the H-K distribution generalizes existing models such as the K-distribution. The H-K distribution models the field of the optical wave as the sum of a deterministic component and a random component, the intensity of which follows the Rice (Nakagami- $n$ ) distribution. The average intensity of the random portion of the field is treated as a fluctuating quantity [19]. It is important to underline that, to the best of our knowledge, so far there are no published papers which have analyzed the performance of FSO systems over such channel conditions, because of the rather complicated mathematical form of their respective probability density functions (PDF).

TABLE I  
LIST OF MATHEMATICAL NOTATIONS USED IN THIS PAPER

$j^2 = -1$ denotes the imaginary unit
$ z $ denotes the magnitude of the complex number $z$
$\Re\{z\}$ denotes the real part of the complex number $z$
$\Im\{z\}$ denotes the imaginary part of the complex number $z$
$f(x) = o[g(x)]$ as $x \rightarrow x_0$ if $\lim_{x \rightarrow x_0} \frac{f(x)}{g(x)} = 0$
$\ \cdot\ _F^2$ denotes the square Frobenius norm
$(\cdot)^T$ denotes the matrix transpose
$*$ denotes convolution
$\mathbb{E}\{\cdot\}$ denotes expectation
$f_X(\cdot)$ denotes the Probability Density Function (PDF) of the random variable $X$
$F_X(\cdot)$ denotes the Cumulative Distribution Function (CDF) of the random variable $X$
$\mathcal{M}_X(\cdot)$ denotes the Moment Generating Function (MGF) of the random variable $X$
$I_a(\cdot)$ is the modified Bessel function of the first kind and order $a$ [1, eq. (8.431)]
$K_a(\cdot)$ is the modified Bessel function of the second kind and order $a$ [1, eq. (8.432)]
$\Gamma(x) = \int_0^\infty \exp(-t)t^{x-1}dt$ is the Gamma function [1, eq. (8.310/1)]
$Q(x) = \frac{1}{\sqrt{2\pi}} \int_x^\infty \exp(-t^2/2)dt$ is the Gauss Q-function
$W_{p,q}(\cdot)$ is the Whittaker function [1, eq. (9.220)]
$\Pr\{\cdot\}$ denotes the probability operator
$\hat{\cdot}$ denotes estimated value at the receiver side

Depending on the type of detection, FSO systems can be classified into two main categories, namely coherent (heterodyne detection) and non-coherent (direct detection) systems. Coherent FSO systems have the information bits encoded directly onto the electric field of the optical beam. At the receiver, a local oscillator (LO) is employed to extract the information encoded on the optical carrier electric field. Coherent FSO systems can provide significant performance enhancements due to spatial temporal selectivity and heterodyne gain in comparison to direct detection systems. Moreover, they are more versatile as any kind of amplitude, frequency, or phase modulation can be employed. However, coherent receivers are more difficult to implement as the LO field should be spatially and temporally coherent with the received field. The performance of coherent FSO systems has been addressed in several research works. Representative examples can be found in [23]–[27] and references therein.

Recently, the so-called optical spatial modulation (OSM) has emerged as a power- and bandwidth-efficient single-carrier transmission technique for optical wireless communication systems [28]–[30]. This spatial diversity scheme, initially proposed in [31] and further investigated in [32]–[34], employs a simple modulation mechanism that foresees to activate just one out of several MIMO transmitters at any time instant and to use the index of the activated transmitter as an additional dimension for conveying implicit information. Recent research studies have pointed out that OSM can increase the data rate by base two logarithm of the number of transmit units [28]. Also, OSM can increase the data rate by two-times and four-times as compared to on-off keying (OOK) and pulse position modulation (PPM), respectively [28], [29]. It is noted that such

performance gains are obtained with a significant reduction in receiver complexity and system design: No synchronization among MIMO elements is necessary and low-complexity non-coherent detection may be used instead of multiple-stream detection, usually employed in conventional MIMO systems [34].

Because of the above mentioned advantages of OSM over other more conventional transmission schemes and given the wide applicability of FSO systems, it is of interest to investigate the potential performance enhancements obtained by incorporating OSM in FSO systems. However, although the performance of indoor OSM has already been assessed in recent research works, to the best of our knowledge, a performance analysis of *outdoor* OSM with coherent detection is not yet available in the open technical literature. Thus this paper presents for the first time a novel and very generic analytical framework which can be used to accurately obtain the performance of outdoor OSM with coherent detection in the presence of turbulence-induced fading. More specifically and within this framework, the main novel contributions of the paper can be summarized as follows:

- New analytical expressions for the ABEP of coherent OSM under turbulence conditions are derived. When the transmitter is equipped with two apertures the resulting analytical expressions are exact, whereas for an arbitrary number of transmit apertures tight upperbounds can be obtained;
- Error performance bounds for coded OSM systems are derived using the transfer function technique [35] and the potential performance enhancements when channel coding is employed are investigated;

Our theoretical analysis is substantiated by means of performance comparisons between extensive numerically evaluated results and equivalent Monte Carlo simulations.

The remainder of this paper is organized as follows. Section II outlines the system and channel models. In Section III analytical expressions for the ABEP of OSM are presented. The performance of coded OSM systems is discussed in Section IV. In Section V the various performance results and their interpretations are presented. Finally, concluding remarks can be found in Section VI. *Notations:* A comprehensive list of all mathematical notations used in this paper appears in Table I.

## II. SYSTEM AND CHANNEL MODEL

In this section, a detailed description of the OSM FSO system model is provided. Moreover, the H-K distribution is introduced and analytical expressions for its parameters in terms of the physical parameters of the turbulence, such as the refractive-index structure parameter, optical wave number, and propagation path length are derived.

### A. Preliminaries

Consider a  $M \times N$  MIMO FSO system with  $M$  transmit units (lasers) and  $N$  coherent receives respectively. It is assumed that the receiving apertures are separated by more than a coherence length to ensure the independency of fading channels.

The basic principle of OSM modulation is as follows [28], [30]:

i) The transmitter encodes blocks of  $\log_2(M)$  data bits into the index of a single transmit unit. Such a block of bits is hereafter referred to as "message" and is denoted by  $b_m$ ,  $\forall m = 1, 2, \dots, M$ . It is assumed that the  $M$  messages are assumed to be transmitted with equal probability by the encoder and that the related transmitted signal is denoted by  $\tilde{E}_m = E_m \exp(j\phi_{b_m})$ ,  $\forall m = 1, 2, \dots, M$ . During a time slot, only one transmitter  $\ell$ , where  $\ell = 1, 2, \dots, M$  is active for data transmission. The information bits are modulated on the electric field of an optical signal beam through an external modulator. At this particular time slot, the remaining transmit lasers are kept silent, i.e. they do not transmit.

ii) At the receiver, the incoming optical field is mixed with a local oscillator (LO) field and the combined wave is first converted by the photodetector to an electrical one. A bandpass filter is then employed to extract the intermediate frequency (IF) component of the total output current. Finally, a  $N$ -hypothesis detection problem is solved to retrieve the active transmit unit index, which results in the estimation of the unique sequence of bits emitted by the transmitter.

### B. Receiver Structure

Let  $b_m$  with  $m = 1, \dots, M$  be the transmitted message. The received electric field at the aperture plane of the  $n$ -th receiver after mixing with a LO beam, can be expressed as

$$e_n(t) = \sqrt{2P_t Z_0} E_m h_{m,n} \cos(\omega_0 t + \phi_{m,n} + \phi_{b_m}) + \sqrt{2P_{LO} Z_0} \cos(\omega_{LO} t) \quad (1)$$

where  $P_t$  is the transmit laser power,  $Z_0$  is the free space impedance,  $h_{m,n}$  and  $\phi_{m,n}$  denote the magnitude and the phase of the complex channel coefficient between the  $m$ -th transmit and the  $n$ -th receive aperture, respectively,  $P_{LO}$  denotes the power of the local oscillator,  $\omega_{LO} \triangleq \omega_0 + \omega_{IF}$  where  $\omega_0$  and  $\omega_{IF}$  are the carrier and the intermediate radian frequencies, respectively.

The output current of the  $n$ -th photodetector can be expressed as

$$i_n(t) = \frac{R}{Z_0} (e_n(t))^2 \quad (2)$$

where  $R = \eta e / (h\nu_0)$  is the responsivity of the photodetector with  $e = 1.6 \times 10^{-19} \text{ Cb}$  is the charge of an electron,  $h = 6.6 \times 10^{-34} \text{ J} \cdot \text{s}$  is the Planck constant,  $\eta$  is the photodetector efficiency, and  $\nu_0 \triangleq \omega_0 / (2\pi)$  is the optical center frequency. Expanding (2) and ignoring the double-frequency terms that are filtered out by the bandpass filter, the resulting photocurrent can be expressed as

$$i_n(t) = RP_t E_m^2 h_{m,n}^2 + RP_{LO} + 2R\sqrt{2P_t P_{LO}} E_m h_{m,n} \cos(\omega_{IF} t - \phi_{m,n} - \phi_{b_m}) \triangleq i_{DC}(t) + i_{AC}(t) \quad (3)$$

In (3),  $i_{DC}(t) \triangleq RP_t E_m^2 h_{m,n}^2 + RP_{LO}$  is the DC component generated by the signal and local oscillator fields, respectively,  $i_{AC}(t) \triangleq 2R\sqrt{2P_t P_{LO}} \cos(\omega_{IF} t - \phi_{m,n} - \phi_{b_m})$  is the AC component in the received photocurrent which, unlike for direct detection, contains information about the frequency and phase of the received signal. It is assumed that for coherent detection the intermediate frequency  $\omega_{IF}$  is nonzero. Consequently, the signal power can be expressed as  $P_s = 2R^2 P_t P_{LO} E_m^2 h_{m,n}^2$ .

Throughout this analysis, it is assumed that  $P_{LO} \gg P_s$  and thus, the DC photocurrent can be approximated as  $i_{DC}(t) \approx RP_{LO}$ . The photodetection process is impaired by shot noise with variance  $\sigma_{\text{shot},L}^2 = 2eRP_{LO}B_e$  where  $B_e$  is the electrical bandwidth of the photodetector. It is also noted that because of the large value of  $RP_{LO}$  the photocurrent due to thermal noise and the dark current can be ignored.

Following [27] and [25], the sufficient statistics at the  $n$ -th coherent receiver can be expressed as

$$y_n = \sqrt{\mu} h_{m,n} E_m \exp[j(\phi_{m,n} + \phi_{b_m})] + z_n \quad (4)$$

where  $\mu = \frac{RP_t}{eB_e}$  is the average electrical signal-to-noise ratio (SNR) and  $z_n$  is the noise at the  $n$ -th receiver. Assuming that the local oscillator power is large and the receiver noise is dominated by local oscillator related noise terms, the Additive White Gaussian Noise (AWGN) model can be employed as an accurate approximation of the Poisson photon-counting detection model [25]–[27]. Thus,  $z_n$  can be modeled as a zero-mean unit variance complex Gaussian random variable [27].

Throughout this work it is assumed that the receiver has knowledge of the actual fading gains. Furthermore, it is assumed that the total fading remains constant over one bit interval and changes from one interval to another in an independent manner. At the receiver, the optimal spatial

modulation detector estimates the active transmitter index,  $\ell$ , at a given time slot according to [36]

$$\begin{aligned}\hat{\ell} &= \underset{\ell}{\operatorname{argmax}} p_{\mathbf{y}}(\mathbf{y}|\mathbf{x}, \mathbf{H}) \\ &= \underset{\ell}{\operatorname{argmin}} \left\{ \sqrt{\mu} \|\mathbf{h}_{\ell} \mathbf{x}_{\ell}\|_F^2 - 2(\mathbf{y}^T \mathbf{h}_{\ell} \mathbf{x}_{\ell}) \right\}\end{aligned}\quad (5)$$

where

- $\mathbf{x}$  is an  $M$ -dimensional vector with elements corresponding to the electrical field  $E_m \exp(j\phi_{b_m})$  that is transmitted over the optical MIMO channel.
- $\mathbf{H}(t)$  is an  $N \times M$  optical MIMO channel defined as

$$\begin{aligned}\mathbf{H}(t) &= [\mathbf{h}_1, \dots, \mathbf{h}_M] \\ &\triangleq \begin{bmatrix} h_{11}(t) \exp(j\phi_{11}) & \dots & h_{1M}(t) \exp(j\phi_{1M}) \\ h_{21}(t) \exp(j\phi_{21}) & \dots & h_{2M}(t) \exp(j\phi_{2M}) \\ \vdots & \ddots & \vdots \\ h_{N1}(t) \exp(j\phi_{N1}) & \dots & h_{NM}(t) \exp(j\phi_{NM}) \end{bmatrix}\end{aligned}\quad (6)$$

- $\mathbf{z}$  is the  $N$ -dimensional noise vector.
- $p_{\mathbf{y}}(\mathbf{y}|\mathbf{x}, \mathbf{H})$  is the PDF of  $\mathbf{y}$  conditioned on the transmitted vector  $\mathbf{x}$  and the channel  $\mathbf{H}$ .

### C. Channel Model

A discrete scattering model is considered, where the radiation field of an optical wave at a particular point is assumed to be composed of a number of scattered components that have traveled different paths. Under the Ricean assumption [19], the complex channel path gains  $\tilde{h}_{ij}(t)$  between the  $i$ -th transmitter and the  $j$ -th photodetector can be expressed as  $\tilde{h}_{ij}(t) = h_{ij}(t) \exp(j\omega t)$  where  $\omega$  is the radian frequency of the optical wave and

$$\begin{aligned}h_{ij}(t) &= \Re\{h_{ij}(t)\} + j\Im\{h_{ij}(t)\} \\ &= A_{ij} \exp[j\theta_{ij}(t)] + R_{ij}(t) \exp[j\Phi_{ij}(t)]\end{aligned}\quad (7)$$

where the term  $A_{ij} \exp(j\theta_{ij}(t))$  is a deterministic component and  $R_{ij}(t) \exp(j\Phi_{ij}(t))$  is a circular complex Gaussian random variable. Hence, the amplitude  $R_{ij}$  is Rayleigh distributed with parameter  $\sigma_{ij}^2 = b_{ij}/2$  [19, Eq. (13)] and the phase  $\Phi_{ij}$  is uniformly distributed over  $[0, 2\pi]$ . Under the assumption of a doubly stochastic scintillation model [19], the effect of random fluctuations in the turbulence parameters is modeled by allowing random variations in the parameter  $b_{ij}$  of the Rayleigh component. Following [19], it is further assumed that  $b_{ij}$  follows a gamma distribution with PDF given by

$$f_{b_{ij}}(b) = \left( \frac{\alpha_{ij}}{b_0} \right)^{\alpha_{ij}} \frac{b^{\alpha_{ij}-1}}{\Gamma(\alpha_{ij})} \exp\left(-\frac{\alpha_{ij}b}{b_0}\right) \quad (8)$$

where  $\alpha$  is the shaping parameter and represent the effective number of scatters and  $b_{0_{ij}} = \mathbb{E}\{b_{ij}\}$ . Then, the PDF of the irradiance  $I_{ij} = |h_{ij}(t)|^2$ ,  $f_{I_{ij}}(I)$ , can be expressed as [19, Eq. (8)]

$$\begin{aligned}f_{I_{ij}}(I) &= \frac{(\alpha_{ij}/b_{0_{ij}})^{\alpha_{ij}}}{\Gamma(\alpha_{ij})} \\ &\times \int_0^\infty b^{\alpha_{ij}-2} \exp\left(-\frac{\alpha_{ij}b}{b_{0_{ij}}} - \frac{I + A_{ij}^2}{b}\right) I_0\left(\frac{2A_{ij}\sqrt{I}}{b}\right) db\end{aligned}\quad (9)$$

which is actually the integral representation of the H-K distribution [18]. It is noted that  $f_{I_{ij}}(I)$  cannot, in general, be expressed in closed form, with the exception of the special cases  $A_{ij} = 0$  or  $\alpha = 1$ . Specifically, for  $A_{ij} = 0$  (9) reduces to the K-distribution whereas for  $\alpha = 1$ , (9) is reduced to a special case of the I-K distribution [18, Eq. (10)].

The  $\nu$ -th normalized moment of  $I_{ij}$  is given by [18, Eq. (22)] as

$$\frac{\mathbb{E}\{I_{ij}^\nu\}}{\mathbb{E}\{I_{ij}\}^\nu} = \frac{\nu!}{\alpha_{ij}^\nu (1 + \rho_{ij})^\nu} \sum_{k=0}^{\nu} \binom{\nu}{k} \frac{\Gamma(\alpha_{ij} + \nu - k)}{\Gamma(\alpha_{ij})} \frac{(\alpha_{ij}\rho_{ij})^\nu}{\nu!} \quad (10)$$

where  $\rho_{ij} = A_{ij}^2/b_{0_{ij}}$  is the coherence parameter, defined as the power ratio of mean intensities of the constant-amplitude component and random component of the field in (7) [19], [20]. Using (10), the *scintillation index* can be readily calculated as

$$\sigma_{I_{ij}}^2 \triangleq \frac{\mathbb{E}\{I_{ij}^2\}}{\mathbb{E}\{I_{ij}\}^2} - 1 = \frac{\alpha_{ij} + 2\alpha_{ij}\rho_{ij} + 2}{\alpha_{ij}(1 + \rho_{ij})^2}. \quad (11)$$

Under the assumption of spherical wave propagation,  $\sigma_{I_{ij}}^2$  can be directly related to atmospheric conditions as [20, Eq. (7), Eq. (9)]

$$\sigma_{I_{ij}}^2 \approx \begin{cases} 0.41\alpha_{ij}2(1 + 0.5\sigma_1^2), & \sigma_1 \ll 1 \\ 1 + 2.8/\sigma_1^{4/5}, & \sigma_1 \gg 1 \end{cases} \quad (12)$$

where  $\sigma_1^2 = 1.23C_{n_{ij}}^2 k^{7/6} L_{ij}^{11/6}$  is the Rytov variance,  $k = 2\pi/\lambda$  is the optical wave number with  $\lambda$  being the wavelength,  $L_{ij}$  is the link distance and  $C_{n_{ij}}$  denotes the index of refraction structure parameter. For FSO links near the ground,  $C_{n_{ij}}^2 \approx 1.7 \times 10^{-14} \text{ m}^{-2/3}$  and  $8.4 \times 10^{-15} \text{ m}^{-2/3}$  for the daytime and night, respectively [37]. Moreover,  $\sigma_1 \ll 1$  and  $\sigma_1 \gg 1$  correspond to weak and strong turbulence conditions, respectively.

Using (12), the parameters of the H-K distribution,  $\alpha$  and  $\rho$ , can be directly related to physical parameters of the turbulence by following a similar line of arguments as in [20], where similar results were derived for the I-K distribution. In particular, on the one hand, weak turbulence conditions are characterized in the H-K distribution by large values of  $\rho_{ij}$ . In this case the scintillation index given by (11) can be approximated as

$$\sigma_{I_{ij}}^2 \approx \frac{2}{\rho_{ij}}, \text{ with } \rho_{ij} \gg 1. \quad (13)$$

On the other hand, assuming strong turbulence conditions where  $\rho_{ij}$  tends to zero, (11) can be approximated as

$$\sigma_{I_{ij}}^2 \approx 1 + \frac{2}{\alpha_{ij}}, \text{ with } \rho_{ij} \ll 1. \quad (14)$$

By comparing (13) and (14) with the first and second branches of (12), respectively,  $\alpha_{ij}$  and  $\rho_{ij}$  can be obtained as

$$\alpha_{ij} = 0.71\sigma_{1_{ij}}^{4/5} \quad (15)$$

$$\rho_{ij} = \frac{4.88}{\sigma_{1_{ij}}^2 (1 + 0.2\sigma_{1_{ij}}^2)} \quad (16)$$

To the best of our knowledge, the relationship of  $\alpha_{ij}$  and  $\rho_{ij}$  with  $\sigma_{1_{ij}}$  given by (15) and (16) is a novel result.

### III. PERFORMANCE ANALYSIS OF UNCODED OSM OVER TURBULENCE CHANNELS

In this section, by employing the well-known MGF-based approach for the performance analysis of digital communications over fading channels [35], analytical expressions for the ABEP of uncoded OSM systems will be derived. Expressions for the diversity and coding gains of OSM systems are also presented, thus providing useful insight as to how these parameters affect system performance.

#### A. Preliminaries

For  $M = 2$ , the conditional bit error probability (BEP) of OSM systems when no turbulence induced fading is considered can be obtained in closed form as [38]

$$P_E(\mathbf{h}_1, \mathbf{h}_2) = Q\left(\sqrt{\frac{\mu}{4}\|\mathbf{h}_1 - \mathbf{h}_2\|_F^2}\right). \quad (17)$$

The squared Frobenius norm in (17) can be expressed as

$$\|\mathbf{h}_1 - \mathbf{h}_2\|_F^2 = \sum_{n=0}^N |h_{1,n} - h_{2,n}|^2 \quad (18)$$

where  $h_{i,n}$  is the  $n$ -th element of  $\mathbf{h}_i$ ,  $\forall i \in \{1, 2\}$ . When  $M > 2$  transmitters are considered, a tight upper bound for the conditional BEP of the above system can be obtained as [28, Eq. (7)]

$$P_E(\mathbf{H}) \leq \frac{M^{-1}}{\log_2(M)} \times \sum_{m_1=1}^M \sum_{m_2 \neq m_1=1}^M N_b(m_1, m_2) \text{PEP}(m_1 \rightarrow m_2) \quad (19)$$

where  $\text{PEP}(m_1 \rightarrow m_2)$  denotes the Pairwise Error Probability (PEP) related to the pair of transmitters  $m_1$  and  $m_2$ , where  $m_1$  and  $m_2 \in \{1, 2, \dots, M\}$ , and  $N_b(m_1, m_2)$  is the number of bit which have occurred when the receiver decides incorrectly that  $m_2$  instead of  $m_1$  has been active. The  $\text{PEP}(m_1 \rightarrow m_2)$  can be evaluated as [28, Eq. (8)]

$$\text{PEP}(m_1 \rightarrow m_2) = Q\left(\sqrt{\frac{\mu}{4}\|\mathbf{h}_{m_1} - \mathbf{h}_{m_2}\|_F^2}\right). \quad (20)$$

#### B. MGF-Based Approach

When atmospheric turbulence is taken into account, the conditional error probabilities in (17) and (19) need to be averaged over the elements of the channel matrix  $\mathbf{H}$  in order to evaluate the ABEP. Without loss of generality, let us consider the case of a  $2 \times N$  MIMO system. Since  $h_{i,n}$  are complex Gaussian random variables, the difference  $\Delta_n \triangleq h_{1,n} - h_{2,n}$  is a complex Gaussian random variable having mean equal to the difference of the means of  $h_{i,n}$  and variance equal to the sum of variances of  $h_{i,n}$ . In order to deduce a closed form expression for the ABEP, it is further assumed that  $h_{i,n}$  have uncorrelated real and imaginary components with the same variance  $\sigma_n^2 = b_n/2$ . It is noted that such an assumption is justified for link distances of the order of km and for aperture separation distances of the order of cm [39]–[41]. For example, in [41] it was reported that for a link distance of 1.5 km, a

wavelength of 1550 nm, an aperture diameter of 1 mm and photodetectors separated by as little as 35 mm, which validates the independence assumption.

Consequently,  $\Delta_n$  has uncorrelated components too and its squared envelope,  $|\Delta_n|^2$ , is characterized by a non-central chi-square PDF as follows

$$f_{|\Delta_n|^2}(x|b_n) = \frac{1}{2b_n} \exp\left(-\frac{x + \tilde{A}_n^2}{2b_n}\right) I_0\left(\frac{\tilde{A}_n \sqrt{x}}{b_n}\right) \quad (21)$$

where  $\tilde{A}_n = |A_{2,n}e^{j\theta_{2,n}} - A_{1,n}e^{j\theta_{1,n}}|$ . Assuming that  $b_n$  follows a gamma distribution with parameters  $\alpha_n$  and  $b_{0,n}$ , the unconditional PDF of  $|\Delta_n|^2$  is obtained by averaging (21) with respect to  $b_n$ , i.e.

$$f_{|\Delta_n|^2}(x) = \frac{(\alpha_n/b_{0,n})^{\alpha_n}}{2\Gamma(\alpha_n)} \times \int_0^\infty b_n^{\alpha_n-2} \exp\left(-\frac{\alpha_n b_n}{b_{0,n}} - \frac{x + \tilde{A}_n^2}{2b_n}\right) I_0\left(\frac{\tilde{A}_n \sqrt{x}}{b_n}\right) db_n \quad (22)$$

As was pointed out in [19], the integral in (22) cannot be solved in closed form. Nevertheless, for the special case of  $\alpha_n = 1$ , i.e. when one scatterer per branch is considered, and by employing [19, Eq. (10)], this integral can be evaluated in closed form as

$$f_{|\Delta_n|^2}(x) = \begin{cases} \frac{1}{b_{0,n}} K_0\left(\sqrt{2\tilde{A}_n/b_{0,n}}\right) I_0\left(\sqrt{2x}/b_{0,n}\right), & x < \tilde{A}_n^2 \\ \frac{1}{b_{0,n}} I_0\left(\sqrt{2\tilde{A}_n/b_{0,n}}\right) K_0\left(\sqrt{2x}/b_{0,n}\right), & x > \tilde{A}_n^2. \end{cases} \quad (23)$$

Moreover, for the special case where  $h_{1,n}$  and  $h_{2,n}$  have identical mean value, i.e. when  $\tilde{A}_n = 0$ , (22) yields the well known K-distribution with PDF given by

$$f_{|\Delta_n|^2}(x) = 2^{(1-\alpha_n)/2} \Gamma(\alpha_n) \left(\frac{\alpha_n x}{b_{0,n}}\right)^{(\alpha_n-1)/2} \times K_{\alpha_n-1}\left(\sqrt{\frac{2\alpha_n x}{b_{0,n}}}\right). \quad (24)$$

By employing the MGF-based approach for the performance analysis of digital communications over fading channels, the average PEP (APEP) can be obtained as

$$\text{APEP} = \frac{1}{\pi} \int_0^{\pi/2} \prod_{n=1}^N \left[ \mathcal{M}_{|\Delta_n|^2}\left(\frac{\mu}{8\sin^2\theta}\right) \right] d\theta. \quad (25)$$

Moreover, using the tight approximation for the Gaussian Q-function presented in [42, Eq. (14)] (i.e.,  $Q(x) \approx \frac{1}{12} \exp(-x^2) + \frac{1}{4} \exp(-2x^2/3)$ ), an expression accurately approximating APEP can be deduced as

$$\text{APEP} \approx \frac{1}{12} \prod_{n=1}^N \left[ \mathcal{M}_{|\Delta_n|^2}\left(\frac{\mu}{8}\right) \right] + \frac{1}{4} \prod_{n=1}^N \left[ \mathcal{M}_{|\Delta_n|^2}\left(\frac{\mu}{6}\right) \right]. \quad (26)$$

In the following analysis, analytical expressions for the MGF of  $|\Delta_n|^2$  will be deduced. Specifically, the following result holds:

**Proposition 1.** An integral representation for the MGF of  $|\Delta_n|^2$  can be deduced as

$$\begin{aligned} \mathcal{M}_{|\Delta_n|^2}(s) &= \frac{(\alpha_n/b_{0,n})^{\alpha_n}}{\Gamma(\alpha_n)} \\ &\times \int_0^\infty \frac{b^{\alpha_n-1}}{2bs+1} \exp\left(-\frac{\tilde{A}_n s}{2bs+1} - \frac{\alpha_n b}{b_{0,n}}\right) db. \end{aligned} \quad (27)$$

*Proof:* By employing the definition of the MGF,  $\mathcal{M}_{|\Delta_n|^2}(s)$  can be obtained as

$$\begin{aligned} \mathcal{M}_{|\Delta_n|^2}(s) &= \int_0^\infty \exp(-sx) f_{|\Delta_n|^2}(x) dx \\ &= \frac{(\alpha_n/b_{0,n})^{\alpha_n}}{2\Gamma(\alpha_n)} \int_0^\infty \int_0^\infty \exp\left(-sx - \frac{\alpha_n b}{b_{0,n}} - \frac{x + \tilde{A}_n^2}{2b}\right) \\ &\times I_0\left(\frac{\tilde{A}_n \sqrt{x}}{b}\right) b^{\alpha_n-2} db dx. \end{aligned} \quad (28)$$

By changing the order of integration, the above equation can be expressed as

$$\begin{aligned} \mathcal{M}_{|\Delta_n|^2}(s) &= \frac{(\alpha_n/b_{0,n})^{\alpha_n}}{2\Gamma(\alpha_n)} \int_0^\infty b^{\alpha_n-2} \exp\left(-\frac{\alpha_n b}{b_{0,n}}\right) \\ &\left[ \int_0^\infty \exp\left(-sx - \frac{x + \tilde{A}_n^2}{2b}\right) I_0\left(\frac{\tilde{A}_n \sqrt{x}}{b}\right) dx \right] db \end{aligned} \quad (29)$$

The inner integral, i.e. with respect to  $x$  can be evaluated by employing [43, Eq. (3.15.2.2)] as

$$\begin{aligned} \int_0^\infty \exp\left(-sx - \frac{x + \tilde{A}_n^2}{2b}\right) I_0\left(\frac{\tilde{A}_n \sqrt{x}}{b}\right) dx &= \\ \frac{2b}{2sb+1} \exp\left[\frac{1}{2\tilde{A}_n b(2sb+1)}\right] \end{aligned} \quad (30)$$

Substituting (30) into (29) and after some straightforward manipulations, (27) is readily deduced thus completing the mathematical proof. ■

The integral in (27) can be accurately approximated by employing a Gauss-Chebyshev Quadrature (GCQ) technique as [44]

$$\begin{aligned} \mathcal{M}_{|\Delta_n|^2}(s) &\approx \frac{(\alpha_n/b_{0,n})^{\alpha_n}}{\Gamma(\alpha_n)} \\ &\times \sum_{j=0}^J w_j \frac{t_j^{\alpha_n-1}}{2t_j s + 1} \exp\left(-\frac{\tilde{A}_n s}{2t_j s + 1} - \frac{\alpha_n t_j}{b_{0,n}}\right) \end{aligned} \quad (31)$$

where  $J$  is the number of integration points,  $t_j$  are the abscissas and  $w_j$  the corresponding weights. In [45, eqs. (22) and (23)],  $t_j$  and  $w_j$  are defined as

$$t_j = \tan\left[\frac{\pi}{4} \cos\left(\frac{2j-1}{2J}\pi\right) + \frac{\pi}{4}\right] \quad (32a)$$

$$w_j = \frac{\pi^2 \sin\left(\frac{2j-1}{2J}\pi\right)}{4J \cos^2\left[\frac{\pi}{4} \cos\left(\frac{2j-1}{2J}\pi\right) + \frac{\pi}{4}\right]}. \quad (32b)$$

For the special case of  $\tilde{A}_n = 0$ , it can be shown that (27) can be evaluated in closed form. Specifically, the following result holds:

**Corollary 1.** For the special case of  $\tilde{A} = 0$  the MGF of  $|\Delta_n|^2$  can be deduced in closed form as

$$\begin{aligned} \mathcal{M}_{|\Delta_n|^2}(s) &= \left(\frac{\alpha_n}{2sb_{0,n}}\right)^{\frac{\alpha_n}{2}} \exp\left(\frac{\alpha_n}{4sb_{0,n}}\right) \\ &\times W_{-\frac{\alpha_n}{2}, \frac{\alpha_n-1}{2}}\left(\frac{\alpha_n}{2sb_{0,n}}\right) \end{aligned} \quad (33)$$

This result can be readily deduced by employing the integral representation of the Whittaker  $W$ -function given in [1, Eq. (9.222)]. Moreover it is worth pointing out that (33) is in agreement with a previously known result, namely the analytical expression for the MGF of the K-distribution. [46, Eq. (4)].

### C. Diversity and Coding Gain Analysis

In order to obtain the diversity and coding gains of the considered OSMMIMO system can be computed by the framework presented in [47] will be followed. In particular, a generic analytical expression, which becomes asymptotically tight at high SNR values, will be derived for the APEP appearing in (25), as follows:

**Proposition 2.** For high SNR values, (25) can be approximated by

$$\text{APEP} \stackrel{\mu \gg 1}{\approx} \frac{2^{N-1} \Gamma(N + \frac{1}{2})}{\sqrt{\pi} \Gamma(N+1)} \left[ \prod_{n=1}^N c_\ell \right] \left(\frac{\mu}{4}\right)^{-N} \quad (34)$$

where

$$c_n = \left(\frac{\tilde{A}_n}{2}\right)^{\frac{\alpha_n-1}{2}} \frac{(\alpha_n/b_{0,n})^{\frac{\alpha_n+1}{2}}}{\Gamma(\alpha_n)} K_{\alpha_n-1} \left(\sqrt{\frac{2\tilde{A}_n \alpha_n}{b_{0,n}}}\right) \quad (35)$$

*Proof:* According to [47, Proposition 3], the asymptotic error performance of the OSM system depends on the behavior of  $\mathcal{M}_{|\Delta_n|^2}(s)$ , as  $s \rightarrow \infty$ . To determine an analytical asymptotic expression for APEP a Taylor series expansion is employed to approximate  $\mathcal{M}_{|\Delta_n|^2}(s)$  as

$$|\mathcal{M}_{|\Delta_n|^2}(s)| = c_n |s|^{-d_n} + o(|s|^{-d_n}), \quad s \rightarrow \infty \quad (36)$$

where  $c_n$  and  $d_n$  are parameters that determine the diversity and coding gains of the  $n$ -th diversity branch, respectively. Observe that since  $\tilde{A}_n/(2sb+1) \stackrel{s \rightarrow \infty}{\approx} \tilde{A}_n/(2b)$  and  $1/(2sb+1) \stackrel{s \rightarrow \infty}{\approx} 1/(2bs)$ , (27) yields

$$\begin{aligned} \mathcal{M}_{|\Delta_n|^2}(s) &\approx \frac{(\alpha_n/b_{0,n})^{\alpha_n}}{2s\Gamma(\alpha_n)} \\ &\times \int_0^\infty b^{\alpha_n-2} \exp\left(-\frac{\tilde{A}_n}{2b} - \frac{\alpha_n b}{b_{0,n}}\right) db. \end{aligned} \quad (37)$$

By employing [43, Eq. (2.2.2.1)], (37) can be solved in closed form yielding

$$\begin{aligned} \mathcal{M}_{|\Delta_n|^2}(s) &\approx \left(\frac{\tilde{A}_n}{2}\right)^{\frac{\alpha_n-1}{2}} \frac{(\alpha_n/b_{0,n})^{\frac{\alpha_n+1}{2}}}{s\Gamma(\alpha_n)} \\ &\times K_{\alpha_n-1} \left(\sqrt{\frac{2\tilde{A}_n \alpha_n}{b_{0,n}}}\right) \end{aligned} \quad (38)$$

By comparing (38) and (36) it is readily deduced that  $d_n = 1$  and  $c_n$  is given by (35). Thus, by substituting (36) into (25), the asymptotic PEP expression can be obtained as in (34) which concludes the proof. ■

From (34) it is clear that the diversity and coding gains achieved by the considered system are  $N$  and  $\prod_{n=1}^N c_n$ , respectively. It is also evident that the diversity gain depends only on the number of the receive apertures and is independent of the fading severity. This finding is in agreement with relevant findings reported in [38] and [48], for the case of radio-frequency MIMO wireless systems.

It is noted that for the special case  $\tilde{A}_n = 0$ , i.e. when  $|\Delta_n|^2$  follows the K-distribution, by employing the asymptotic result  $K_t(x) \xrightarrow{x \rightarrow 0} \frac{\Gamma(t)}{2} \left(\frac{2}{x}\right)^t$  [44],  $c_n$  can be further simplified as

$$c_n = \frac{\alpha_n}{2b_{0,n}(\alpha_n - 1)}. \quad (39)$$

#### IV. PERFORMANCE ANALYSIS OF CODED OSM OVER TURBULENCE CHANNELS

##### A. Preliminaries

When coded OSM is employed, the input signal  $\mathbf{s}(t)$  is first encoded by a convolutional encoder. The encoded data are interleaved by a random block interleaver and transmitted through the optical wireless channels using spatial modulation. It is also assumed that perfect interleaving at the transmitter and de-interleaving at the receiver is used. Assuming maximum likelihood soft decision decoding, the log likelihood ratios (LLRs) for the  $i$ -th constellation bit when the  $\ell$ -th transmitting antenna is active are computed as [28, Eq. (6)]

$$\begin{aligned} \text{LLR} &= \log \frac{\Pr\{\ell^i = 1 | \mathbf{y}\}}{\Pr\{\ell^i = 0 | \mathbf{y}\}} \\ &= \log \frac{\sum_{\hat{\ell} \in \mathcal{L}_1^i} \exp\left(-\frac{\|\mathbf{y} - \mathbf{h}_{\hat{\ell}} s_{\ell}\|^2}{N_0}\right)}{\sum_{\hat{\ell} \in \mathcal{L}_0^i} \exp\left(-\frac{\|\mathbf{y} - \mathbf{h}_{\hat{\ell}} s_{\ell}\|^2}{N_0}\right)} \end{aligned} \quad (40)$$

where  $\mathcal{L} \in \{1 : M\}$  is the set of spatial constellation points,  $\mathcal{L}_1^i$  and  $\mathcal{L}_0^i$  are subsets from  $\mathcal{L}$  containing the transmitter indices having "1" and "0" at the  $i$ -th bit, respectively. The resulting data are finally decoded by a Viterbi decoder.

##### B. Performance Analysis

A union bound on the ABEP of a coded communication system can be evaluated as [35]

$$\bar{P}_{\text{ub}} \leq \frac{1}{n} \sum_{\mathbf{X}} P(\mathbf{X}) \sum_{\mathbf{X} \neq \mathbf{X}'} q(\mathbf{X}, \mathbf{X}') \text{PEP}(\mathbf{X}, \mathbf{X}') \quad (41)$$

where  $P(\mathbf{X})$  is the probability that the coded sequence  $\mathbf{X}$  is transmitted,  $q(\mathbf{X}, \mathbf{X}')$  is the number of information bit errors in choosing another coded sequence  $\mathbf{X}'$  instead of  $\mathbf{X}$   $n$  is the number of information bits per transmission and  $\text{PEP}(\mathbf{X}, \mathbf{X}')$  is the pairwise error probability, i.e. the probability of selecting  $\mathbf{X}'$  when  $\mathbf{X}$  was actually transmitted.

By employing [35, p. 510], (41) can be efficiently evaluated as

$$\bar{P}_{\text{ub}} \leq \frac{1}{n} \sum_{\mathbf{X}} P(\mathbf{X}) \int_0^{\pi/2} \left[ \frac{\partial}{\partial N} T[D(\theta), N] \Big|_{N=1} \right] \quad (42)$$

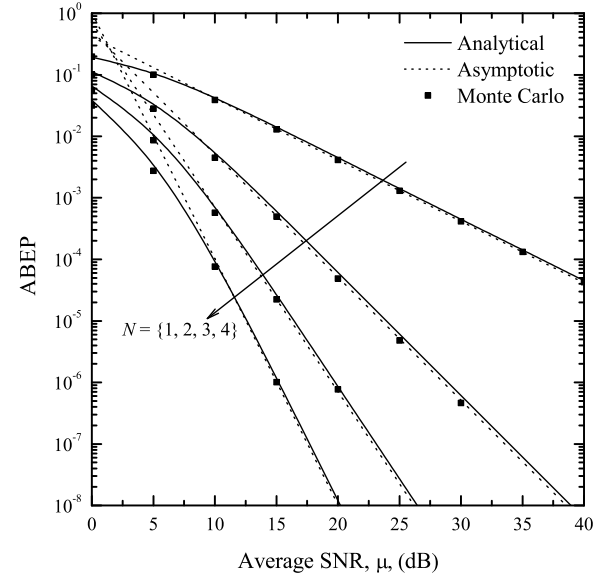


Fig. 1. ABEP of uncoded OSM for  $2 \times N$  MIMO H-K turbulent channels as a function of the average SNR,  $\mu$ , for various number of receiving apertures,  $N$ . Simulation Parameters:  $A_{1,n} = 2$ ,  $A_{2,n} = 1$ ,  $\theta_{1,n} = \pi/3$ ,  $\theta_{2,n} = \pi/4$ ,  $\alpha_n = 2$ ,  $b_{0,n} = 2$ .

where  $T[D(\theta), N]$  is the transfer function of the employed convolutional code,  $N$  is an indicator variable taking into account the number of the erroneous bits and  $D(\theta)$  depends on the underlying PEP expression. Furthermore, assuming that uniform error probability (UEP) codes are considered and taking into account the symmetry property this code family exhibits, thus making the distance structure of a UEP code independent of the transmitted sequence, (42) can be further simplified as [35]

$$\bar{P}_{\text{ub}} \leq \frac{1}{\pi} \int_0^{\pi/2} \left[ \frac{1}{n} \frac{\partial}{\partial N} T[D(\theta), N] \Big|_{N=1} \right]. \quad (43)$$

For  $M = 2$ , using (17), (18) and the Craig's formula for the Gauss Q-function, i.e.  $Q(x) = 1/\pi \int_0^{\pi/2} \exp(-x^2/2 \sin^2 \theta) d\theta$ ,  $D(\theta)$  can be obtained as

$$D(\theta) = \prod_{n=1}^N \mathcal{M}_{|\Delta_n|^2} \left( \frac{\mu}{8 \sin^2 \theta} \right) \quad (44)$$

where  $\mathcal{M}_{|\Delta_n|^2}$  can be obtained from (27). When  $M > 2$ , by employing [28, Eq. (13)], and using a similar line of arguments as in the case of  $M = 2$ ,  $D(\theta)$  can be obtained by

$$\prod_{m_1=1}^M \prod_{m_2 \neq m_1}^M \mathcal{M}_{|\Delta_{m_1, m_2}|^2} \left( \frac{\mu}{8 \sin^2 \theta} \right) \quad (45)$$

where  $|\Delta_{m_1, m_2}|^2 = \|\mathbf{h}_{m_1} - \mathbf{h}_{m_2}\|^2$ . The last MGF can be easily computed analytically with the help of (27).

#### V. PERFORMANCE EVALUATION RESULTS AND DISCUSSION

In this section the various performance evaluation results which have been obtained using by numerically evaluating the mathematical expressions presented in Sections III, IV

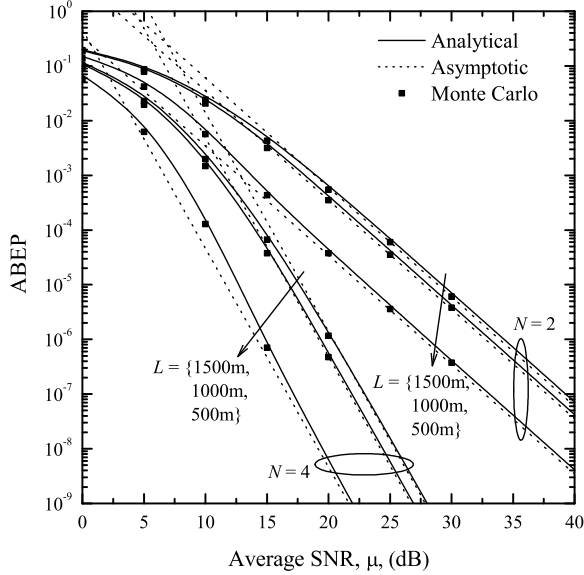


Fig. 2. ABEP of uncoded OSM for  $2 \times 2$  and  $2 \times 4$  MIMO H-K turbulent channels as a function of the average SNR,  $\mu$ , for various values of link distances,  $L$ . Simulation Parameters:  $\lambda = 1550\text{nm}$ ,  $C_n^2 = 1.7 \times 10^{-14}\text{m}^{-2/3}$ ,  $\theta_{1,n} = \pi/3$ ,  $\theta_{2,n} = \pi/4$ .

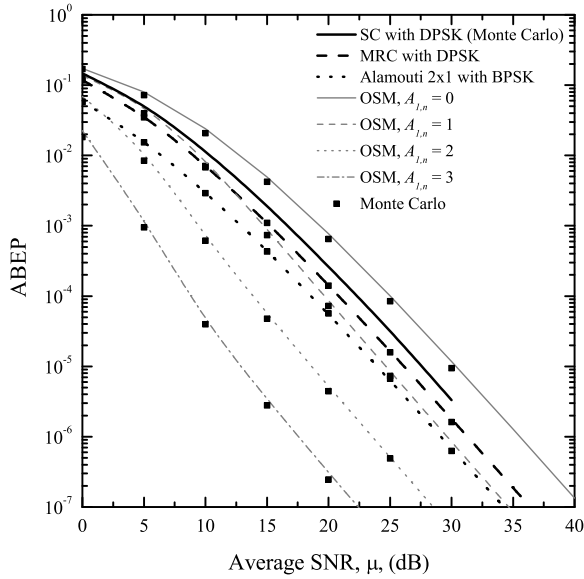


Fig. 3. ABEP Comparison of  $2 \times 2$  OSM with  $1 \times 2$  coherent MRC systems employing DPSK, as a function of the average SNR,  $\mu$ , for various values of  $A_{1,n}$ . Simulation Parameters:  $A_{2,n} = 0$ ,  $\theta_{1,n} = 0$ ,  $\theta_{2,n} = 0$ ,  $\alpha_n = 1.5$ ,  $b_{0,n} = 1.5$ .

for uncoded and coded OSM systems operating over H-K turbulent channels will be presented. In particular, for uncoded OSM systems the following performance evaluation results will be presented: *i*) ABEP vs. SNR for  $2 \times N_r$  OSM systems (obtained using (26) with (27), and (34) - see Figs. 1, 2 and 3); *ii*) ABEP vs. SNR for  $2 \times N$  MIMO OSM systems,  $2 \times N$  MIMO (obtained using (26) with (27)). For the uncoded schemes, in order to validate the accuracy of the previously mentioned expressions, comparisons with complementary Monte Carlo simulated performance results are also included in these figures. As far as the performance

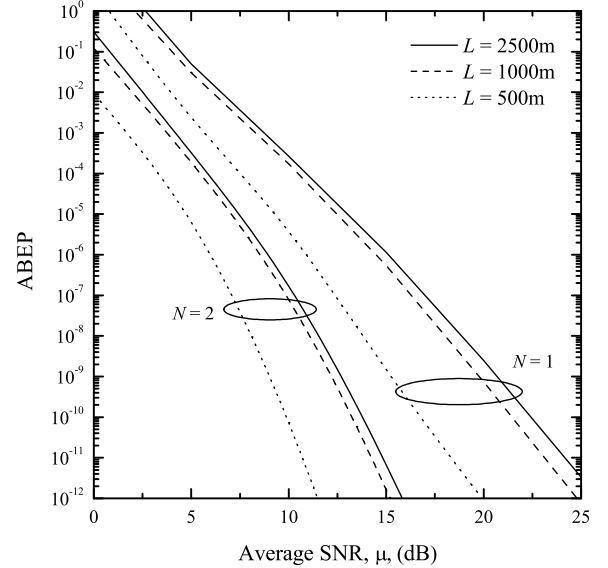


Fig. 4. ABEP upper bounds of coded OSM for  $2 \times 2$  and  $2 \times 1$  H-K turbulent channels as a function of the average SNR,  $\mu$ , for various values of link distances,  $L$ . Simulation Parameters:  $\lambda = 1550\text{nm}$ ,  $C_n^2 = 1.7 \times 10^{-14}\text{m}^{-2/3}$ ,  $\theta_{1,n} = \pi/3$ ,  $\theta_{2,n} = \pi/4$ .

of coded OSM systems is concerned, ABEP upper bounds vs. SNR have been obtained using (43) with (27) (see Fig. 4).

Fig. 1, presents ABEP as a function of the average electrical SNR,  $\mu$ , of  $2 \times N$  MIMO OSM systems with  $N \in \{1, 2, 3, 4\}$ . Independent and identically distributed branches are considered with  $A_{1,n} = 2$ ,  $A_{2,n} = 1$ ,  $\theta_{1,n} = \pi/3$ ,  $\theta_{2,n} = \pi/4$ ,  $\alpha_n = 2$ ,  $b_{0,n} = 2$ . The obtained results clearly indicate that the ABEP approximation curves, obtained using (26), are in close agreement with those obtained via simulations, verifying the correctness of the proposed analysis. Moreover, it is evident that the asymptotic ABEP curves correctly predict the diversity and coding gains of the considered system for all tested cases.

In Fig. 2, the dependence on the link distance  $L$  of the ABEP of a  $2 \times N$  MIMO OSM system is illustrated. The considered system is again equipped with either  $N = 2$  or  $N = 4$  receiving apertures and identically distributed branches are assumed. The parameters of the H-K distribution are calculated from (15) and (16) assuming spherical wave propagation. Following [49], it is further assumed that the operating wavelength is  $\lambda = 1550\text{ nm}$  and  $C_n^2 = 1.7 \times 10^{-14}\text{m}^{-2/3}$ . As expected, the error performance deteriorates as  $L$  increases from  $L = 500\text{m}$  to  $L = 1500\text{m}$ . Moreover, it is evident that an increase in  $L$  from  $500\text{m}$  to  $1000\text{m}$  results in a more severe performance deterioration than in the case where  $L$  increases from  $1000\text{m}$  to  $1500\text{m}$ . In all considered cases the analytical results, obtained using (26), are compared with the equivalent results obtained via Monte-Carlo simulations and, as it is evident, similar findings to the one reported in the previous test cases can be verified.

In the following analysis, OSM is compared with coherent  $1 \times M$  systems employing either Maximal Ratio Combining (MRC) or Selection Combining (SC) diversity reception and Differential Phase Shift Keying (DPSK) as well as with the  $2 \times 1$  coherent transmit diversity scheme employing Alamouti

space time coding and Binary Phase Shift Keying (BPSK), proposed in [26]. The instantaneous SNR at the output of the coherent MRC receiver assuming equal average SNR per receiving aperture,  $\mu$  can be expressed as

$$\gamma_{\text{MRC}} = \mu \sum_{n=1}^N I_n. \quad (46)$$

whereas for SC it can be expressed as

$$\gamma_{\text{SC}} = \max\{\mu I_1, \mu I_2\} \quad (47)$$

The conditioned on the fading intensity bit error probability of the coherent DPSK FSO system can be expressed as [23]

$$P(e|I) = \frac{1}{2} \exp(-\gamma_{\text{MRC,SC}}). \quad (48)$$

When MRC is employed, the ABEP can be deduced as [35]

$$P_E = \frac{1}{2} \prod_{n=1}^N \mathcal{M}_{I_n}(\mu). \quad (49)$$

In the SC case, an analytical expression for the ABEP is more difficult to be deduced and, therefore, ABEP will be evaluated by means of Monte Carlo simulation only. Finally, following [26], the instantaneous SNR at the input of the demodulator of the Alamouti-type optical receiver has a similar form as Eq:MRC. For this scheme, the ABEP of BPSK can be evaluated as

$$P_E = \frac{1}{\Pi} \int_0^{\pi/2} \prod_{n=1}^N \mathcal{M}_{I_n} \left( \frac{\mu}{\sin^2 \theta} \right) d\theta. \quad (50)$$

In order to simplify the underlying mathematical analysis, it is assumed that the PDF of  $I_n$  is given by (9) with the parameters  $A_n$  being all zero, i.e. the PDF is the K-distribution. Thus,  $\mathcal{M}_{I_n}(\mu)$  can be readily obtained in closed form from (33) by replacing  $b_{0,n}$  with  $b_{0,n}/2$ . In Fig. 3, the ABEP of  $2 \times 2$  MIMO OSM links is compared with the ABEP of  $1 \times 2$  coherent FSO systems with DPSK. Throughout this test case, identically distributed links are considered. In order to compare these systems under the same propagation conditions, it is assumed that  $\alpha_n = 1, 5$ ,  $b_{0,n} = 1.5$ ,  $A_{2,n} = 0$  and various values of  $A_{1,n} = 0$ . As it can be observed, when either MRC or SC are employed, coherent DPSK performs worse than OSM for values of  $A_{1,n}$  up to approximately 1, however it outperforms OSM at lower values of  $A_{1,n}$ . Moreover, OSM outperforms the Alamouti scheme for  $A_{1,n} = 2$  and 3 and exhibits similar performance for high SNR values when  $A_{1,n} = 1$ . For  $A_{1,n} = 1$  and lower values of  $A_{1,n}$  the Alamouti scheme yields the best performance of the considered OSM schemes. When more transmit apertures are employed, however, this advantage is compensated by the superior spectral efficiency of OSM and its lower hardware complexity compared to coherent MRC. Specifically, OSM offers increased spectral efficiency by a factor  $\log_2(M)$  [28]. Moreover, as only one transmitting aperture is activated at any symbol duration, OSM has a lower decoding complexity compared to conventional MRC and Alamouti schemes.

In Fig. 4, upper bounds on the error probability of coded  $2 \times 1$  and  $2 \times 1$  OSM systems are depicted, assuming

similar propagation conditions to those considered in Fig. 2. Throughout this analysis, a convolutional code with rate 1/3 and constraint length of 3 is considered. The transfer function of this code is given as [50, Eq. (8.2.6)]

$$T[D(\theta), N] = \frac{D(\theta)^6 N}{1 - 2ND(\theta)^2}. \quad (51)$$

Substituting (51) to (43), a union bound on the ABEP can be obtained as

$$\bar{P}_{\text{ub}} \leq \frac{1}{\pi \log_2(M)} \int_0^{\pi/2} \frac{D(\theta)^6}{(1 - 2D(\theta)^2)^2} d\theta. \quad (52)$$

The performance results of Fig. 4 clearly show that, as expected, the incorporation of convolutional coding significantly enhances the performance of OSM systems, even when a small number of receive apertures is employed, even for  $N = 1$ .

## VI. CONCLUSION

In this paper, the use of spatial modulation technique for FSO communication systems has been proposed. We have provided a comprehensive analytical framework for error performance analysis in the presence of atmospheric turbulence scattering channel models which include the H-K distribution. The proposed framework reveals important information about the performance of OSM over such turbulent channels, including the effect of fading severity and the achievable diversity and coding gains, and provides valuable insight into the impact of channel parameters on performance of OSM. Upper bounds for the ABEP performance of coded OSM systems have also been derived, demonstrating that coding techniques can greatly enhance the performance of OSM. An extensive simulation campaign has been conducted to validate the proposed mathematical framework and the obtained analytical expressions. Important trends about the performance of OSM for a variety of atmospheric turbulent scenarios and MIMO setups have also been demonstrated. Specifically, it was shown that OSM can provide significant performance enhancements in the presence of atmospheric turbulence, comparable to the ones offered by conventional coherent systems with spatial diversity, while outperforming the latter in terms of spectral efficiency and hardware complexity. Besides, under specific propagation conditions, OSM can yield better performance than conventional SIMO systems employing MRC or SC. The proposed framework is also useful for understanding the performance trend, important properties and tradeoffs of outdoor OSM operating in the presence of atmospheric turbulence. Moreover, it can serve as an efficient tool to the system design engineer for performance analysis and system optimization purposes.

## REFERENCES

- [1] I. Gradshteyn and I. M. Ryzhik, *Tables of Integrals, Series, and Products*, 6th ed. New York: Academic Press, 2000.
- [2] X. Zhu and J. M. Kahn, "Free-space optical communications through atmospheric turbulence channels," *IEEE Transaction on Communications*, vol. 50, no. 8, pp. 1293–1300, 2002.
- [3] A. K. Majumdar, "Free-space laser communication performance in the atmospheric channel," *L. Opt. Fiber Commun. Rep.*, vol. 2, pp. 345–396, 2005.

- [4] Z. Ghassemlooy and W. Popoola, "Terrestrial free-space optical communications," in *Mobile and Wireless Communications: Network Layer and Circuit Level Design*. InTech, 2010.
- [5] S. G. Wilson, M. Brandt-Pearce, Q. Cao, and J. H. Leveque, "Free-space optical MIMO transmission with Q-ary PPM," *IEEE Trans. Commun.*, vol. 53, no. 8, pp. 1402–1412, Aug. 2005.
- [6] A. Garcia-Zambrana, "Error rate performance for STBC in free-space optical communications through strong atmospheric turbulence," *IEEE Commun. Lett.*, vol. 11, no. 5, pp. 390–392, May 2007.
- [7] N. Letzepis and A. Fabregas, "Outage probability of the free space optical channel with doubly stochastic scintillation," *IEEE Trans. Commun.*, vol. 57, no. 10, pp. 2899–2902, Oct 2009.
- [8] S. M. Navidpour, M. Uysal, and M. Kavehrad, "Performance of free-space optical transmission with spatial diversity," *IEEE Trans. Wireless Commun.*, vol. 6, no. 8, pp. 2813–2819, Aug. 2007.
- [9] C. Castillo-Vazquez, A. Garcia-Zambrana, and B. Castillo-Vazquez, "Closed-form BER expression for FSO links with transmit laser selection over exponential atmospheric turbulence channels," *Electr. Lett.*, vol. 23, no. 45, 2009.
- [10] M. Safari and M. Uysal, "Do we really need space-time coding for free-space optical communication with direct detection," *IEEE Trans. Wireless Commun.*, vol. 7, no. 11, pp. 4445–4448, Nov. 2008.
- [11] Z. Wang, W.-D. Zhong, S. Fu, and C. Lin, "Performance comparison of different modulation formats over free-space optical (FSO) turbulence links with space diversity reception technique," *IEEE Photonics Journal*, vol. 1, no. 6, pp. 277–285, Dec 2009.
- [12] T. A. Tsiftsis, H. G. S sandalidis, G. K. Karagiannidis, and M. Uysal, "Optical wireless links with spatial diversity over strong atmospheric turbulence channels," *IEEE Trans. Wireless Commun.*, vol. 8, no. 2, pp. 951–957, 2009.
- [13] K. Peppas, "A simple, accurate approximation to the sum of gamma-gamma variates and applications in MIMO free-space optical systems," *IEEE Photon. Technol. Lett.*, vol. 23, no. 13, pp. 839–841, Jul 2011.
- [14] K. Peppas, F. Lazarakis, A. Alexandridis, and K. Dangakis, "Simple, accurate formula for the average bit error probability of multiple-input multiple-output free-space optical links over negative exponential turbulence channels," *Optics Letters*, vol. 37, pp. 3243–3245, Aug. 2012.
- [15] L. C. Andrews, M. A. Al-Habash, C. Y. Hopen, and R. L. Phillips, "Theory of optical scintillation: Gaussian beam wave model," *Waves in Random Media*, vol. 11, pp. 271–291, 2001.
- [16] M. A. Al-Habash, L. C. Andrews, and R. L. Phillips, "Mathematical model for the irradiance PDF of a laser beam propagating through turbulent media," *Opt. Eng.*, vol. 40, no. 8, pp. 1554–1562, 2001.
- [17] J. H. Churnside and S. F. Clifford, "Log-normal Rician probability density function of optical scintillations in the turbulent atmosphere," *Journal of Optical Society of America*, vol. 4, pp. 1923–1930, 1987.
- [18] E. Jakeman, "On the statistics of k-distributed noise," *J. Phys. A*, vol. 13, pp. 31–48, 1980.
- [19] L. C. Andrews and R. L. Phillips, "Mathematical genesis of the I-K distribution for random optical fields," *Journal of the Optical Society of America A*, vol. 3, no. 11, pp. 1912–1919, 1986.
- [20] L. C. Andrews, R. L. Phillips, and K. Shivamoggi, "Relations of the parameters of the I-K distribution for irradiance fluctuations to physical parameters of the turbulence," *Applied Optics*, vol. 27, no. 11, pp. 2150–2155, 1988.
- [21] K. P. Peppas, A. N. Stassinakis, G. K. Topalis, H. E. Nistazakis, and G. S. Tombras, "Average capacity of optical wireless communication systems over I-K atmospheric turbulence channels," *J. Opt. Commun. Netw.*, vol. 4, pp. 1026–1032, 2012.
- [22] H. E. Nistazakis, A. D. Tsigopoulos, M. P. Hanias, C. D. Psychogios, D. Marinos, C. Aidinis, and G. S. Tombras, "Estimation of outage capacity for free space optical links over I-K and K turbulent channels," *Radioengineering*, vol. 20, no. 2, pp. 493–498, 2011.
- [23] K. Kiasaleh, "Performance of coherent DPSK free-space optical communication systems in k-distributed turbulence," *IEEE Trans. Commun.*, vol. 54, no. 4, pp. 604–607, Apr. 2006.
- [24] M. Niu, J. Cheng, and J. F. Holzman, "Error rate analysis of m-ary coherent free-space optical communication systems with k-distributed turbulence," *IEEE Trans. Commun.*, vol. 59, pp. 664–668, Mar. 2011.
- [25] S. M. Aghajanzadeh and M. Uysal, "Diversity-multiplexing trade-off in coherent free-space optical systems with multiple receivers," *IEEE/OSA J. Opt. Commun. Netw.*, vol. 2, pp. 1087–1094, Dec. 2010.
- [26] M. Niu, J. Cheng, and J. F. Holzman, "Alamouti-type STBC for atmospheric optical communication using coherent detection," *IEEE Photonics Journal*, 2014.
- [27] E. Bayaki and R. Schober, "Performance and design of coherent and differential space-time coded FSO systems," *Journal of Lightwave Technology*, vol. 30, no. 11, pp. 1569–1577, Jun. 2012.
- [28] R. Mesleh, H. Elgala, and H. Haas, "Optical spatial modulation," *J. Opt. Commun. Netw.*, vol. 3, no. 3, pp. 234–244, Mar. 2011.
- [29] R. Mesleh, H. Elgala, R. Mehmood, and H. Haas, "Performance of optical spatial modulation with transmitters-receivers alignment," *IEEE Commun. Lett.*, vol. 15, no. 1, pp. 79–81, Jan. 2011.
- [30] T. Fath and H. Haas, "Performance comparison of MIMO techniques for optical wireless communications in indoor environments," *IEEE Trans. Commun.*, vol. 61, no. 2, pp. 733–742, Feb. 2013.
- [31] Y. A. Chau and S.-H. Yu, "Space modulation on wireless fading channels," in *Proc. IEEE Veh. Technol. Conf. Fall*, vol. 3, 2001, pp. 1668–1671.
- [32] R. Y. Mesleh, H. Haas, S. Sinanovic, C. Ahn, and S. Yun, "Spatial modulation," *IEEE Trans. Veh. Technol.*, vol. 57, pp. 2228–2241, Jul. 2008.
- [33] R. Mesleh, M. D. Renzo, H. Haas, and P. M. Grant, "Trellis coded spatial modulation," *IEEE Trans. Wireless Commun.*, vol. 9, no. 7, pp. 2349–2361, Jul. 2010.
- [34] M. D. Renzo, H. Haas, A. Ghayeb, S. Sugiura, and L. Hanzo, "Spatial Modulation for Generalized MIMO: Challenges, Opportunities, and Implementation," *Proc. IEEE*, 2013.
- [35] M. K. Simon and M. S. Alouini, *Digital Communication over Fading Channels*, 2nd ed. New York: Wiley, 2005.
- [36] J. Jegathanan, A. Ghayeb, and L. Szczerzinski, "Spatial modulation: optimal detection and performance analysis," *IEEE Commun. Lett.*, vol. 12, no. 8, pp. 545–547, 2008.
- [37] J. W. Goodman, *Statistical Optics*. John Wiley and Sons, 1985.
- [38] M. D. Renzo and H. Haas, "Space Shift Keying (SSK) MIMO over correlated Rician fading channels: Performance analysis and a new method for transmit-diversity," *IEEE Trans. Commun.*, vol. 59, no. 1, pp. 116–129, Jan. 2011.
- [39] E. Lee and V. Chan, "Part 1: optical communication over the clear turbulent atmospheric channel using diversity," *IEEE J. Sel. Areas Commun.*, vol. 22, pp. 1896–1906, Nov. 2004.
- [40] E. Bayaki, R. Schober, and R. Mallik, "Performance analysis of MIMO free-space optical systems in gamma-gamma fading," *IEEE Trans. Commun.*, vol. 57, no. 11, pp. 3415–3424, Nov. 2009.
- [41] N. Letzepis, I. Holland, and W. Cowley, "The Gaussian free space optical MIMO channel with Qary pulse position modulation," *IEEE Trans. Wireless Commun.*, vol. 7, pp. 1744–1753, May 2008.
- [42] M. Chiani, D. Dardari, and M. K. Simon, "New exponential bounds and approximations for the computation of error probability in fading channels," *IEEE Trans. Wireless Commun.*, vol. 2, pp. 840–845, Jul. 2003.
- [43] A. P. Prudnikov, Y. A. Brychkov, and O. I. Marichev, *Integrals and Series Volume 4: Direct Laplace Transforms*, 1st ed. CRC, 1992.
- [44] M. Abramovitz and I. Stegun, *Handbook of Mathematical Functions with Formulas, Graphs, and Mathematical Tables*. New York, ISBN 0-486-61272-4: Dover, 1964.
- [45] F. Yilmaz and M.-S. Alouini, "An MGF-based capacity analysis of equal gain combining over fading channels," in *Proc. IEEE PIMRC*, Sep. 2010, pp. 945–950.
- [46] P. Theofilakos, A. G. Kanatas, and G. P. Efthymoglou, "Performance of generalized selection combining receivers in  $K$  fading channels," *IEEE Commun. Lett.*, vol. 12, no. 11, pp. 816–818, Nov. 2008.
- [47] Z. Wang and G. Giannakis, "A simple and general parametrization quantifying performance in fading channels," *IEEE Trans. Commun.*, vol. 51, no. 8, pp. 1389–1398, Aug. 2003.
- [48] M. D. Renzo and H. Haas, "Bit error probability of space modulation over Nakagami- $m$  fading: Asymptotic analysis," *IEEE Commun. Lett.*, vol. 15, no. 10, pp. 1026–1028, Oct. 2011.
- [49] M. Uysal, J. T. Li, and M. Yu, "Error rate performance analysis of coded free-space optical links over gamma-gamma atmospheric turbulence channels," *IEEE Trans. Wireless Commun.*, vol. 5, no. 6, pp. 1229–1233, Jun. 2006.
- [50] J. G. Proakis, *Digital Communications*, 3rd ed. New York: Mc Graw Hill, 1995.